Graphene-Assisted Solution Growth of Vertically Oriented Organic Semiconducting Single Crystals

Yue Wang,[†] Jaime A. Torres,[†] Adam Z. Stieg,[†,‡] Shan Jiang,[†] Michael T. Yeung,[†] Yves Rubin,[†] Santanu Chaudhuri,[§] Xiangfeng Duan,[†] and Richard B. Kaner*[,†]

[†]Department of Chemistry and Biochemistry and the California NanoSystems Institute, University of California, Los Angeles, Los Angeles, California 90095-1569, United States, [‡]WPI Center for Materials Nanoarchitectonics, National Institute for Materials Science, Tsukuba, Ibaraki 305-0040, Japan, and [§]Applied Research Institute and Computational Science and Engineering, College of Engineering, University of Illinois at Urbana—Champaign, Champaign, Illinois 61820, United States

ABSTRACT

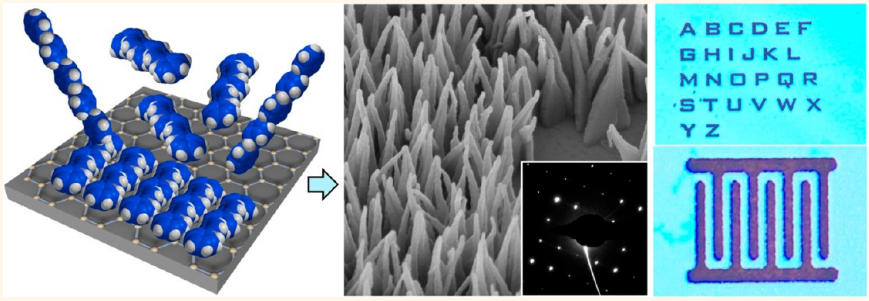

Vertically oriented structures of single crystalline conductors and semiconductors are of great technological importance due to their directional charge carrier transport, high device density, and interesting optical properties. However, creating such architectures for organic electronic materials remains challenging. Here, we report a facile, controllable route for producing oriented vertical arrays of single crystalline conjugated molecules using graphene as the guiding substrate. The arrays exhibit uniform morphological and crystallographic orientations. Using an oligoaniline as an example, we demonstrate this method to be highly versatile in controlling the nucleation densities, crystal sizes, and orientations. Charge carriers are shown to travel most efficiently along the vertical interfacial stacking direction with a conductivity of 12.3 S/cm in individual crystals, the highest reported to date for an aniline oligomer. These crystal arrays can be readily patterned and their current harnessed collectively over large areas, illustrating the promise for both micro- and macroscopic device applications.

KEYWORDS: graphene · oligoaniline · vertical alignment · organic single crystal · selective growth patterning

Conjugated materials including semiconducting or conducting polymers and small molecules have garnered a tremendous amount of attention in recent years largely due to their tunable electronic properties and mechanical flexibility.[1,2] In particular, solution-processable conjugated organic materials hold great promise for next-generation electronic and optoelectronic devices because of their compatibility with low-cost solution processing methods such as spray-coating and roll-to-roll printing.[3] Single crystals of these materials are of particular interest, as they possess the long-range order necessary to allow the intrinsic transport limits to be realized.[4] To achieve large area, high-density device arrays with high throughput, it is crucial to align these single crystals.[4−6]

Various approaches for aligning single crystals oriented parallel with respect to the substrate have led to groundbreaking performances in devices that require 1-D or 2-D transport, such as field-effect transistors.[4,5,7] On the other hand, for applications that benefit from high surface area and directional transport in the vertical direction such as solar cells and sensors, it is desirable to orient the single crystals in the vertical direction (with respect to the substrate) in high density.[8−12] A myriad of "top-down" and "bottom-up" techniques have been developed to achieve such vertical orientation for inorganic materials. Various fields

* Address correspondence to kaner@chem.ucla.edu.

Received for review June 8, 2015 and accepted August 24, 2015.

Published online August 31, 2015
10.1021/acsnano.5b03465

including photovoltaics, vertical transistor arrays, energy-storage devices, self-powered generators, and intercellular interfacing have benefited greatly from these structures and have resulted in technological breakthroughs.[8,13−16] However, approaches for creating such structures for organic materials remain sparse and rely mainly on the guidance of an external porous template.[17−19] These processes generally require harsh conditions for template removal, which are detrimental to the delicate conjugated organic materials, in order to liberate the vertical arrays. Hence, it is highly desirable to develop a method free of porous templates for producing vertically oriented single crystals for soluble conjugated materials.

Graphene has emerged as a good substrate for dictating the orientations of organic molecules on top and have sparked a number of studies in recent years. Various reports have found that conjugated materials, both small molecules[20−26] and polymers,[27,28] tend to orient favorably in a lying down, face-on configuration with respect to graphene due to van der Waals interactions and preferred orbital, electronic density and dipole overlap, as opposed to the more commonly observed standing up, edge-on scenario on other substrates. Such orientation has been shown to enhance device performance for applications such as thin film vertical field-effect transistors.[28−30] Furthermore, owing to its high conductivity, the graphene layer can serve as a good electrode for direct integration into devices.[28,29]

With our growing understanding of the interaction between graphene and conjugated molecules, it is evident that graphene can serve as an effective guiding substrate for vertical growth of conjugated materials. So far, reported organic/graphene heterostructures are largely limited to atomic layers or thin sheets that are most suitable for probing fundamental properties or 2-D devices.[20−30] A recent study using physical vapor deposition to realize vertical organic nanowire arrays on graphene has experimentally illustrated the advantages of having high density 3-D structures for applications such as solar cells.[31] However, the main attractive feature of conjugated materials as opposed to their inorganic counterparts is their low-cost solution processability.[3,4] Hence, a solution-based method for growing high quality, vertically oriented single crystals is highly desirable and poised to advance the current technology of organic electronics.

Here, we describe a simple yet effective solution-based, highly controllable approach for the "bottom-up" growth of vertically oriented single crystal arrays of various conjugated materials on graphene. The crystal arrays possess excellent morphological and crystallographic orientation with the most efficient $\pi-\pi$ stacking carrier transport direction perpendicular to the graphene substrate, a desirable feature for applications such as solar cells, sensors, and supercapacitors. Furthermore, the direct "bottom-up" growth provides intimate contact and extended π-orbital overlap between the crystals and underlying graphene, leading to an unprecedented conductivity of 12.3 S/cm for tetraaniline **1** (a model compound in this study) along the interfacial stacking direction, which is 1 order of magnitude greater than the highest previously reported value.

RESULTS AND DISCUSSION

Phenyl/phenyl-capped tetraaniline (TANI) **1** was chosen as a representative molecule for exploring graphene-assisted vertical crystallization since its monodispersity allows TANI to serve as a good model system for the crystallization of polyaniline, a benchmark conducting polymer.[32−34] The chemical structures of TANI and all other molecules presented here can be found in the Supporting Information. In the crystallization process, a loosely covered container is filled with a nonsolvent for TANI, such as *n*-hexane. A TANI solution is dropped onto a SiO_2/Si substrate coated with a single layer of chemical vapor deposited (CVD) graphene[35] raised above the *n*-hexane liquid level (Figure 1a). The vapor of the nonsolvent saturates the closed chamber and infiltrates into the TANI solution, resulting in supersaturation that induces crystallization. The crystallization event is illustrated in Figure S1. At the end of the process, dark colored TANI can be observed localized over the graphene-covered area, while the bare SiO_2 area remains intact (Figure 1b). A cross-polarized optical micrograph further illustrates the high nucleation affinity of TANI for graphene as evidenced by a sharp interface between the graphene and SiO_2 surfaces where the strongly birefringent TANI crystals are only observed on graphene (Figure 1c). Scanning electron microscopy (SEM) analysis reveals that the crystals are oriented vertically with respect to graphene and exhibit uniform morphological orientation and height (Figure 1d and Figure S2). The nucleation density of these crystals can be readily controlled by varying the solution concentration (Figure 2a). As the solution concentration increases, the crystal deposition density increases steadily. Figure 2b shows a collection of SEM images offering a top view of the crystal arrays achieved with the indicated concentration of TANI dissolved in 2-propanol. The highest concentration tested here is 2.0 mg/mL, which is slightly below the saturation value of TANI in 2-propanol.

To decipher the crystallographic information, several crystals were transferred to transmission electron microscopy (TEM) grids for selected area electron diffraction (SAED) analysis. The electron diffraction pattern of a plate laying flat on a TEM grid (Figure 3a) shows sharp Bragg spots, indicating that these plates are single crystals. A (020) *d*-spacing of 0.39 nm is obtained, suggesting that the TANI molecules π-stack parallel to the graphene substrate along the long-axis

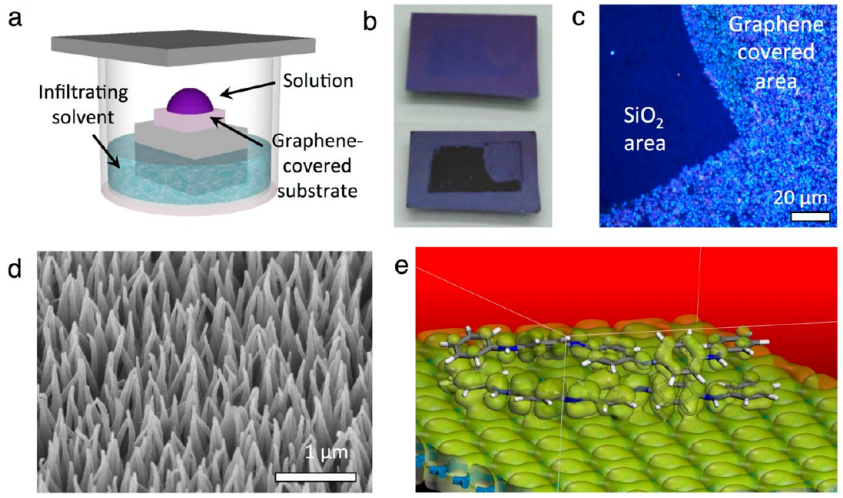

Figure 1. (a) Vapor-infiltration setup used for the experiments. (b) A graphene-coated SiO_2/Si wafer before (top panel) and after (bottom panel) the crystallization of TANI. (c) Polarized optical microscope image showing the SiO_2/graphene interface where crystals only grow on the graphene-covered areas. (d) SEM image showing that the plate-shaped TANI crystals are oriented vertically on graphene. (e) DFTB modeling illustrates the electron density overlap between two TANI molecules and graphene leading to the preferred face-on orientation.

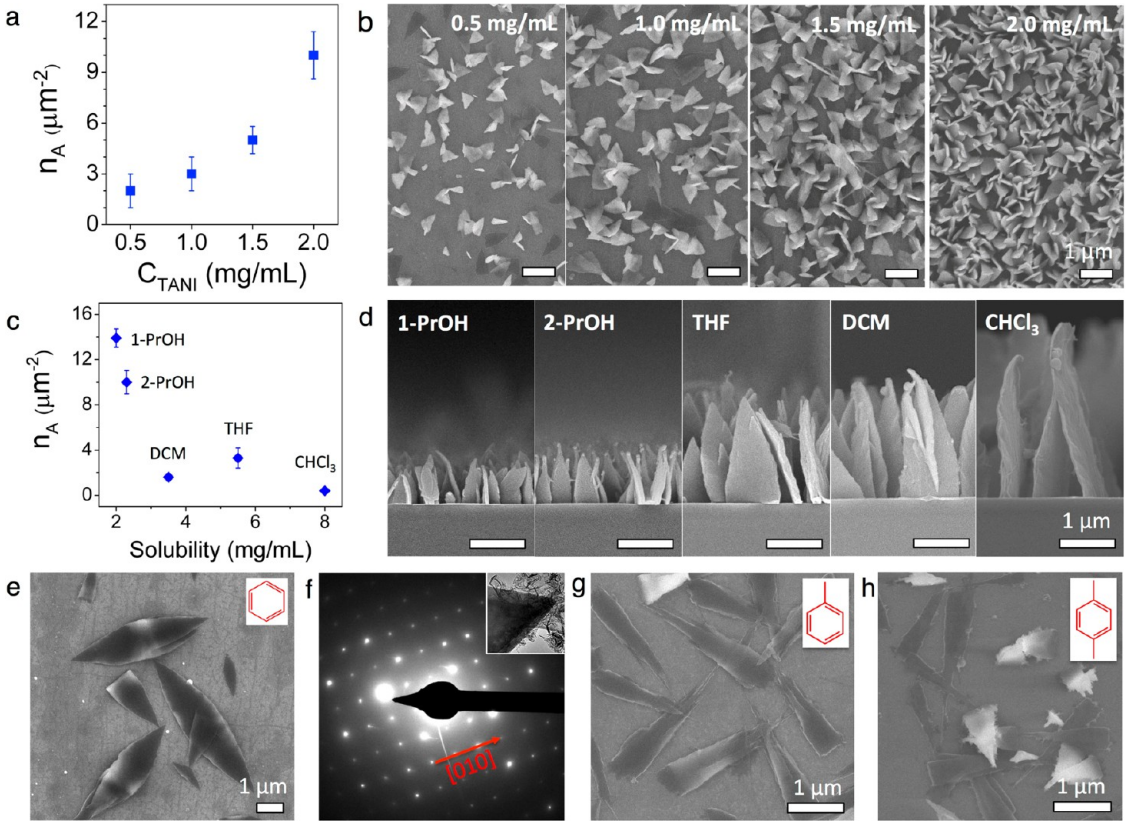

Figure 2. (a) Correlation between solution concentration (C_{TANI}) and crystal nucleation density (n_A). (b) Top-view SEM images showing the different nucleation densities at different concentrations. (c) Correlation between solubility and nucleation density (n_A) of the crystals. (d) Side-view SEM images illustrating the size control of the crystals achieved by using different solvents at a constant concentration of 2 mg/mL. (e–h) Control over the orientation of TANI crystals on graphene: horizontal crystals are obtained by using an aromatic infiltrating solvent; for instance, benzene (e), toluene (g), and *p*-xylene (h). Molecular structures for these solvents are shown as insets on the corresponding SEM image (f) SAED pattern for a crystal from panel e.

of the crystals. In combination with the cross-sectional SAED pattern (Figure 3b), a packing model can be proposed for TANI on graphene with the (100), (010), and (001) *d*-spacings of 0.68, 0.78, and 2.40 nm, respectively (Figure 3e and Supporting Information Figure S4).

When a large-area crystal array (~1 cm^2) was analyzed by powder XRD, only one intense peak at 23.8° 2θ,

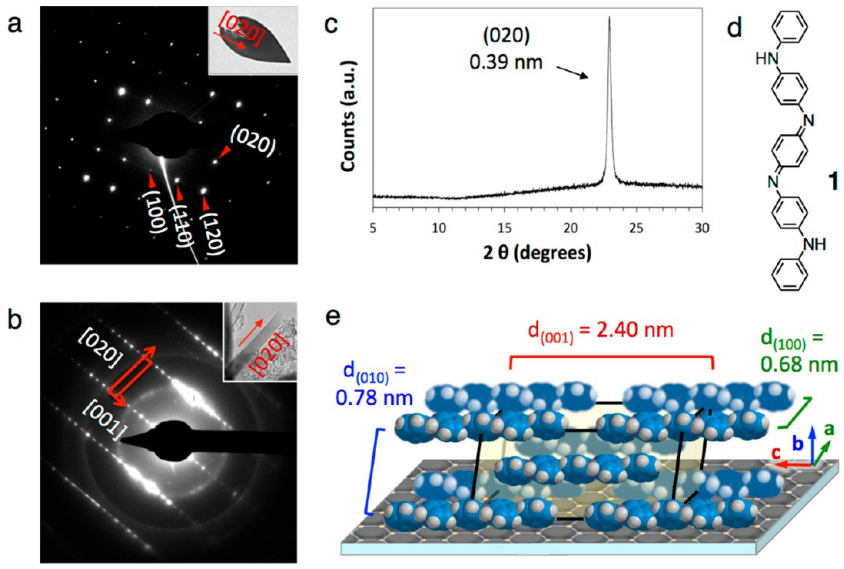

Figure 3. Crystallographic characteristics of the TANI plates: (a and b) Top-view and side-view (respectively) electron diffraction patterns of the vertical plates (with corresponding images shown in inset) transferred to a TEM grid. (c) Powder XRD pattern of the crystal arrays. (d) Molecular structure of TANI; (e) proposed packing arrangement for the TANI crystals obtained from SAED data. The back layer of molecules along the *a*-axis is represented in a different shade of color for clarity.

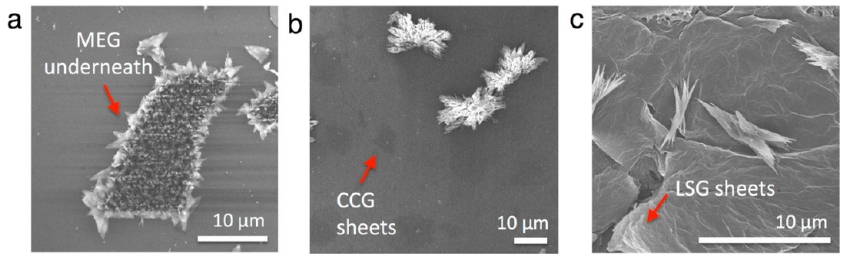

Figure 4. TANI crystals grown on different types of graphene: (a) vertically oriented crystals grow selectively on mechanically exfoliated graphene (MEG) sheets; however, only clusters of crystals are obtained on (b) chemically converted graphene (CCG) and (c) laser scribed graphene (LSG) with no selectivity for these graphene covered areas *vs* the SiO_2 substrate.

corresponding to 0.39 nm, was observed (Figure 3c). This value is in agreement with the (020) spacing obtained from SAED, which indicates that all molecules are uniformly π-stacked along the vertical direction in each crystal over a large area. These results suggest that unlike the conventional template-guided methods, which provide alignment for a supramolecular morphology yet offer little control over the molecular packing direction,[17−19] our graphene-assisted approach exerts both excellent morphological and crystallographic orientational control. For anisotropic materials such as organic semiconductor crystals, uniform orientation in solid-state packing is crucial for achieving stable and consistent device performance at the macroscopic scale toward important applications such as solar cells and sensors.[8−10]

To understand the mechanism behind the graphene-assisted crystallization, we performed experimental and theoretical investigations into (1) the surface requirements, (2) the energetics in binding affinity, and (3) the influence of the solvent system.

To exploit the surface requirement, mechanically exfoliated graphene (MEG),[36] chemically converted graphene (CCG),[37] and laser scribed graphene (LSG)[38] were transferred onto SiO_2/Si substrates for TANI crystallization, to compare with CVD-grown graphene[35] (Figure 4). Among these, oriented vertical crystal arrays grow selectively on the mechanically exfoliated graphene flakes (Figure 4a), in a fashion identical to that on CVD graphene. On the other hand, clusters of crystals with random orientations form when CCG or LSG serve as the substrate (Figure 4b,c, respectively), similar to crystallization on conventional surfaces such as SiO_2. The crystallization does not show any selectivity in nucleation sites when either CCG or LSG and SiO_2 surfaces are present. It has been well established that both CVD-grown and peeled graphene possess a fully sp^2 conjugated carbon lattice,[35,36,39] whereas a small amount of oxygenated groups remain on the basal plane of the graphene sheets formed by reduction of graphene oxide either chemically (CCG) or photothermally (LSG).[37,38] Therefore, an atomically

TABLE 1. Solvent Properties for Vertical Crystallization of TANI

solvent	dielectric[a] constant	relative[b] polarity	boiling[b] point (°C)	vapor[b] pressure (mmHg)	orientation[b]
chloroform	4.8	25.9	61.2	210	vertical
tetrahydrofuran	7.6	20.7	66.0	200	vertical
dichloromethane	9.1	31.0	39.6	350	vertical
2-propanol	18.3	54.6	82.5	44	vertical
1-propanol	20.1	61.7	97.0	21	vertical
acetone	20.6	35.5	56.2	240	random
ethanol	22.4	65.4	78.5	59	random
methanol	32.6	76.2	64.6	128	random
acetonitrile	37.5	46.0	81.6	97	random
dimethyl sulfoxide	46.6	44.4	189.0	0.7	random

[a] Solvents with a dielectric constant lower than 20.1 leads to TANI crystals growing vertically, while those with dielectric constant higher than 20.6 results in clusters of crystals randomly deposited on both graphene and SiO_2 areas. [b] Other solvent properties including boiling point, vapor pressure, and surface tension do not appear to have a controlling effect on the orientation of crystal growth.

homogeneous and defect-free sp^2 hybridized surface is crucial for achieving vertical crystallization of conjugated compounds such as TANI. It provides preferred orbital, electronic density and dipole overlap at the interface between the substrate and the molecules, which have been demonstrated to be crucial factors for controlling the orientation of organic molecules adsorbed on a substrate.[20,21] In fact, tight-binding density functional theory (DFTB) calculations indicate that TANI adsorbs on graphene favorably in a face-on orientation (Figure 1e). This configuration provides the strongest overlap of π-electron densities between the two, while minimizing the repulsive interactions. The binding energy is calculated to be 68 kcal/mol, which indicates an off-centered overlap of the π-electrons of graphene and TANI. Since the preferred orientation between TANI and graphene is face-on, and crystals of conjugated molecules tend to grow along their $\pi-\pi$ stacking direction, TANI crystals grow vertically from the graphene-coated substrate with the $\pi-\pi$ stacking direction perpendicular to graphene.

In addition to surface and energetic factors, both the solvation and infiltrating solvents play important roles in dictating the preferred nucleation and controlling the orientation of TANI crystal growth on graphene. TANI is soluble in a variety of polar solvents. These solutions were cast onto graphene-coated SiO_2/Si substrates for crystallization (Table 1). We observed that when the solvent has a dielectric constant[40] that is less than or equal to that of 1-propanol, arrays of vertical crystals form selectively on the graphene-coated area (Table 1 and Figure S5). On the other hand, when the solvation solvent's dielectric constant[40] is greater than that of 1-propanol, randomly oriented clusters of crystals form all over the substrate, without selectivity for the graphene-coated area (Table 1 and Figure S6). Since graphene is a nonpolar, low surface energy substrate,[41] solvents with lower dielectric constant (*e.g.*, THF) are favorable for achieving thorough wetting, which enables preferred nucleation on graphene when TANI reaches supersaturation. Conversely, more polar solvents (*e.g.*, acetonitrile) do not favorably wet the graphene surface. In fact, as the solvent evaporates, the remaining droplet tends to migrate away from graphene to the higher surface energy SiO_2 area. As a result, large clusters of crystals form on the SiO_2 substrate, while the deposition density on graphene remains low.

The solvation solvent also offers control over the nucleation density and crystal size of the vertical crystals, as shown in Figure 2d and Figure S5, with larger crystals corresponding to lower nucleation density, and smaller ones to higher nucleation density. Plotting the solubility of TANI in these solvents against their nucleation density reveals a nearly inverse proportional relationship (Figure 2c). Since the TANI concentration is close to saturation in solvents such as 1-propanol or 2-propanol, supersaturation is reached soon after *n*-hexane begins to infiltrate, resulting in rapid nucleation that leads to a larger number of smaller crystals. Conversely, a longer nonsolvent infiltration period is needed to induce supersaturation for solvent systems in which TANI is more soluble (*i.e.*, CH_2Cl_2, THF, chloroform). Therefore, a slower nucleation process is created, which leads to larger crystals with lower nucleation densities.[42]

The ability to manipulate crystal orientations on a certain substrate is crucial for expanding the realm of device applications. Here, we demonstrate that the orientation of the TANI crystals on graphene can be controlled by the choice of infiltrating solvents. Hydrocarbon infiltrating solvents with suitable solvation properties lead to vertical crystal growth (Figure S7, S9); however, aromatic infiltrating solvents result in TANI crystal growth in a horizontal orientation, that is, parallel to the graphene substrate (Table S1). Figure 2 panels e, g, and h illustrate the morphology and orientation of TANI crystals with benzene, toluene, and *p*-xylene as infiltration solvents, respectively, while 2-propanol remains as the solvation solvent. The crystals show similar triangle-like morphology as those grown using hydrocarbon infiltrating solvents, but lie

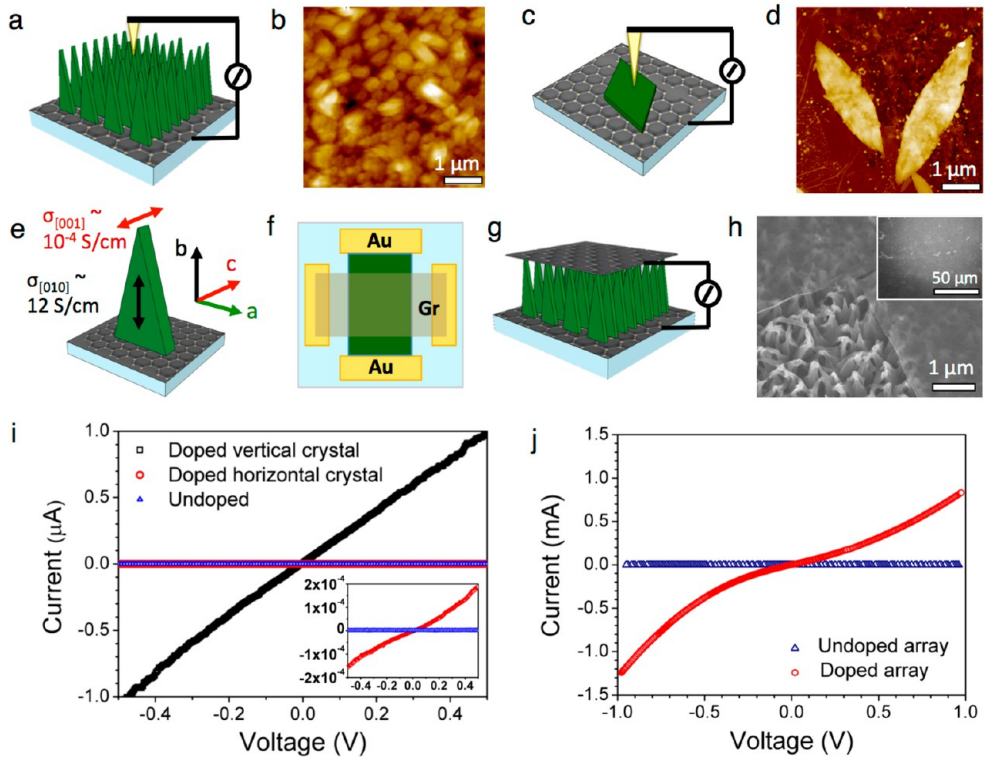

Figure 5. Anisotropic electrical properties of the TANI crystals grown on graphene. (a) Schematic of the conductive-AFM measurement setup for the vertical crystals probing current along the *b*-axis. (b) Topographic AFM image of a high density array of the TANI vertical crystals. (c) Schematic of the conductive-AFM measurement setup for the horizontal crystals where the transport along the *c*-axis can be obtained. (d) Topographic AFM image of a crystal laying horizontally on graphene. (e) Different conductivity values along the different crystallographic axes. (f and g) Schematics showing the top view (f) and the cross-sectional view (g) of the graphene/TANI array/graphene (Gr/TANI/Gr) sandwich device. (h) SEM image showing the top graphene electrode laminated on top of the vertical crystals at an edge of the levitated graphene. Inset illustrates the continuous coverage of the top graphene layer on TANI arrays. (i) Typical *I*−*V* curves obtained for undoped crystals, a single vertical plate, and a single horizontal plate after vapor doping. Inset has a smaller current scale (but same units) showing the lower current for the horizontal plates. (j) *I*−*V* plots of the Gr/TANI/Gr sandwiched devices showing the current scale to be magnitudes higher than that of a single TANI crystal.

horizontally on the graphene substrates. SAED patterns of such crystals reveal the $\pi-\pi$ stacking direction to be along their long-axis, which is now parallel with respect to graphene (inset to Figure 2e). Identical *d*-spacings are observed in the SAED patterns comparable to their vertically oriented counterparts (shown in Figure 3a), indicating the same crystal structure. As shown by the DFTB calculations (Figure 1e), the vertical growth of the conjugated TANI crystals is likely due to the strong affinity for the molecules to bind in a face-on configuration with respect to graphene as a result of the strong electron density overlap. However, aromatic molecules such as benzene also have a high binding affinity for graphene. DFTB calculations show that benzene adsorbs strongly on the graphene surface with an energy of ~17 kcal/mol per benzene molecule. The nucleation sites available for TANI depend on the surface coverage level. At even a quarter of monolayer coverage of a graphene surface by benzene, the probability of TANI adsorbing in a face-on configuration is severely reduced. Although TANI is adsorbed at 68 kcal/mol per molecule according to DFTB calculations, the kinetics of face-on adsorption becomes unfavorable due to the high solvent-to-TANI ratio. Thus, TANI molecules stack more favorably in an edge-on fashion, which in turn alters the crystal growth direction and leads to the horizontal orientation. Note that a small amount of vertically grown crystals are observed when *p*-xylene is used as the infiltrating solvent (Figure 2h). With the two methyl substituents on the benzene ring, it is likely that xylene does not interact with graphene as strongly as the unsubstituted benzene or the monosubstituted toluene, hence allowing for some π-interactions between TANI and graphene which leads to vertical growth.

Control over the TANI crystal orientation on graphene offers the opportunity to examine its anisotropic electrical transport properties along different crystallographic axes. Using the measurement geometry depicted in Figure 5 panels a and c, transport properties along the interfacial stacking direction (*i.e.*, the *b*-axis) and oligomer backbone (*i.e.*, the *c*-axis) can be measured using conductive atomic force microscopy (cAFM), respectively. Topographic AFM images of vertical and horizontal crystals on graphene shown in Figure 5b,d, respectively, enabled precise positioning

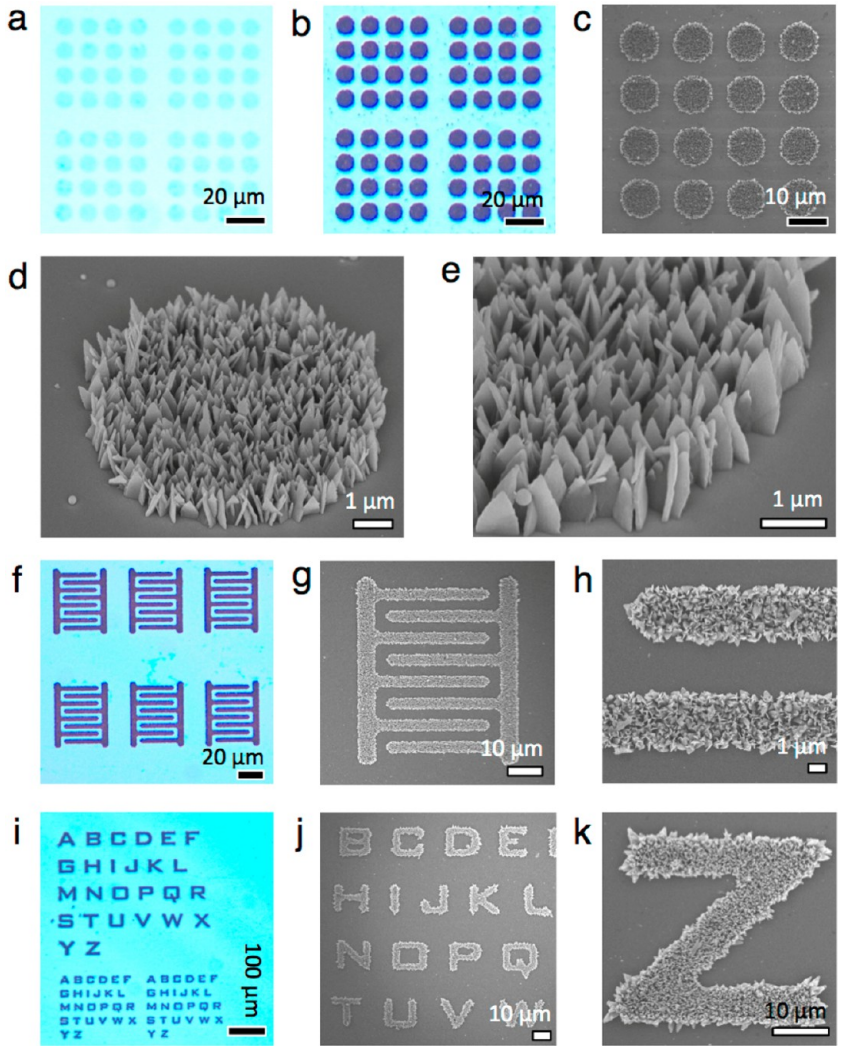

Figure 6. Patterning of vertical organic crystal arrays. (a) Optical microscope images of patterned graphene on a SiO_2/Si substrate. The darker blue circles are graphene. (b) Same substrate after crystallization. TANI crystals only grow on the circular-shaped graphene, leaving the SiO_2 area intact. (c) SEM image of a 4 × 4 circle pattern array showing the high selectivity of the growth location. (d) Tilted view of an array of vertical crystals arranged in the shape of the graphene substrate. (e) A magnified view of a corner of the circle in image d. (f) Optical microscope image of TANI vertical crystal arrays grown in the shapes of interdigitated electrodes. (g and h) Top view SEM images offering a more magnified view of the patterns comprising vertical arrays. (i–k) Optical microscope and SEM images showing the crystal arrays patterned into shapes of letters.

of the top cAFM tip electrode for electrical characterization as well as a direct measure of cross-sectional heights employed in subsequent analyses.

Current–voltage (*I*–*V*) characteristics acquired via cAFM are shown in Figure 5i. An insulating baseline was obtained for the as-grown, undoped crystals regardless of orientation. Upon acid doping (*i.e.*, HCl vapor),[43] the measured current increased by over 6 orders of magnitude for the vertically oriented crystals, corresponding to a conductivity of ~12.3 S/cm (see Figure S10 for cAFM analysis and S11–12 for detailed calculations). The conductivity of horizontal crystals is seen to be significantly lower than that observed for their vertical counterparts (Figure 5i and inset), and is at most ~1.06×10^{-4} S/cm (see Figure S12 for details). Therefore, the conductivity along the interfacial stacking *b*-axis of the oligomer crystals is at least 5 orders of magnitude higher than that along the backbone *c*-axis direction (Figure 5e). The observed anisotropic transport in TANI crystals is most likely a result of the different conduction mechanisms operating along the various crystallographic orientations. Because of the short conjugation length of TANI, the carrier transport along the molecule's backbone is limited and relies on a hopping mechanism between molecules.[44–46] In contrast, the extended conduction network comprising π-orbital overlap is more efficient, therefore leading to a higher conductivity.[47,48] The fact that the vertical direction is the most efficient conduction pathway with a high conductivity renders these structures important for applications that can benefit from directional 3-D

transport such as organic solar cells, batteries, or sensors.[10,49,50]

Furthermore, conductivity along the π-stacked *b*-axis (12.3 S/cm) is 1 order of magnitude higher than the highest previously reported value for tetraaniline (1.1 S/cm),[33] which can be largely attributed to the high-quality interfacial contact and extensive π-orbital overlap created by the direct growth of TANI crystals on graphene. This is in contrast to the bottom-contact configuration typically used for organic nanoscale architecture measurements, where the electrode/crystal interface is known to be nonideal because of solvent impurity traps and the poor contact quality. As a reference, vertical plates grown on graphene were transferred onto bottom-contact microelectrodes for *I*−*V* measurements, and a maximum conductivity of 1.9 S/cm was obtained along the *b*-axis, illustrating the significance of direct growth of conjugated molecules on graphene. It should also be noted that the phenyl/phenyl-capped TANI has greater molecular symmetry when compared to that capped with phenyl/amine from previous studies,[33] which could reduce the number of positional, *cis-trans* and conformational isomers and lead to a more ordered packing.[51] However, since (1) single crystals of these two molecules exhibit conductivity values on the same order of magnitude using bottom-contact measurements (1.9 S/cm vs 1.1 S/cm) and (2) DFT calculations at the B3LYP/6-31G(d) level show negligible differences in the overall distributions of the HOMO coefficients (Figures S13−S14), we conclude that the high conductivity observed here is mainly a result of the intimate contact quality and extensive π-orbital overlap between TANI crystals and graphene.

To harness the current for multiple vertical crystals collectively, another layer of graphene can be laminated on top of the crystal arrays to produce a graphene/TANI/graphene (Gr/TANI/Gr) sandwich structure (Figure 5f,g, Figure S15a). SEM images in Figure 5h illustrate the continuous graphene top electrode levitated over the crystal arrays. *I*−*V* curves in Figure 5j show that prior to acid doping, an insulating baseline is obtained, indicating that the top and bottom layers of graphene are separated by the undoped crystal arrays. Once doped, approximately 1.25 mA of current are detected at an applied voltage of 1.0 V. The current scale for the arrays is 3 orders of magnitude higher than that of a single vertical crystal measured by cAFM, indicating that the vertical crystals sandwiched between graphene are indeed connected in parallel where their current can be harnessed collectively, illustrating the potential of such a structure for large-area device applications.

The patterning of electronic materials is crucial for defining device position, downsizing component dimensions, and minimizing interdevice cross-talk.[52−54] Unfortunately, it is often challenging to apply conventional lithography for patterning organic materials due to their sensitivity to the harsh processing conditions involved in typical lithography processes.[4,7] Therefore, there is considerable interest in the patterning of organic materials through selective growth. Here, by taking advantage of the high nucleation selectivity TANI exhibits for graphene, the deposition locations of TANI crystals can be precisely controlled simply by patterning the graphene substrates. Figure 6a shows an optical micrograph of graphene dots that are 10 μm in diameter patterned *via* photolithography. After the TANI crystallization, only the area covered by the graphene dots has turned dark, indicative of TANI binding (Figure 6b). Top- and tilted-view SEM images further illustrate the high selectivity that TANI crystals have for graphene, evident by the sharp interface and their vertical orientation (Figure 6c−e). Other patterns of vertically oriented TANI crystal arrays, such as interdigitated electrodes, letters, *etc*., can also be readily created by patterning graphene into such shapes at desired locations (Figure 6f−k and Figure S16). Since the photolithography step is carried out before the TANI crystallization process, this approach is completely benign toward the intrinsic properties of conjugated materials and can lead to exciting opportunities for the fabrication of novel organic electronic devices.

This graphene-assisted vertical crystallization method is also widely applicable to other soluble

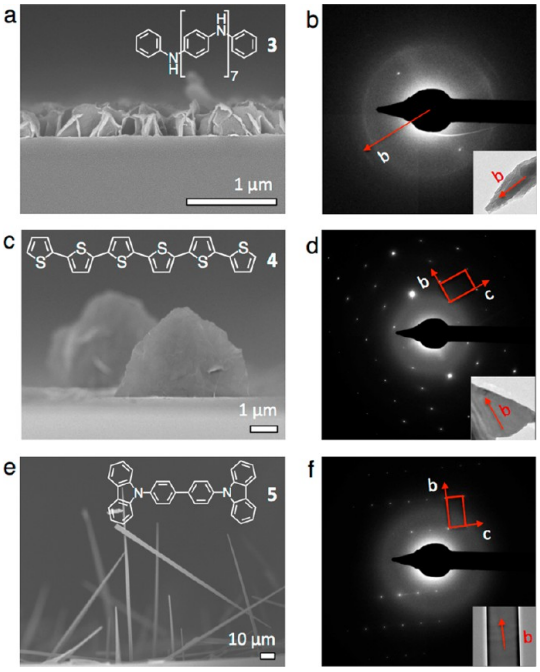

Figure 7. Vertical crystallization of other soluble conjugated compounds on graphene. (a) Vertically oriented octaaniline 3 plates. (b) SAED pattern of a single octaaniline 3 plate showing the preferred packing orientation. (c) Sexithiophene 4 vertical plates. The density of the plates is low because of the poor solubility of sexithiophene 4 in virtually all solvents. (d) Spot pattern from the SAED of a sexithiophene 4 plate illustrates it is a single crystal. (e) Vertical wires of bis(*N*-carbazolyl) biphenyl 5. (f) The corresponding SAED pattern shows that each wire is a single crystal.

conjugated materials. As a proof-of-concept, using the solvent-annealing method and the solvent systems demonstrated in Figure 2d and Table 1, vertically oriented crystal arrays of phenyl/phenyl-capped octaaniline **3** (Figure 7a), sexithiophene **4** (Figure 7c), and bis(*N*-carbazolyl) biphenyl **5** (Figure 7e) have been produced on graphene. The former two exhibit plate-like morphology, while the latter appears as 1-D wires. The corresponding SAED patterns for the vertical crystals are shown in Figure 7 panels b, d, and f. The interfacial stacking distances for these three crystals are 0.38, 0.39, and 0.37 nm, respectively, and all are oriented along their crystal long-axis. The octaaniline **3** plates exhibit arc SAED patterns, indicating that the longer chain length renders the molecule more conformationally flexible, thus introducing packing misorientation. However, sharp Bragg spots are obtained for both sexithiophene **4** and bis(*N*-carbazolyl) biphenyl **5** crystals under SAED analysis, demonstrating their single-crystalline nature. Therefore, graphene-assisted crystallization can be a general approach to obtaining vertically oriented arrays of a wide variety of soluble conjugated materials. With graphene also conveniently serving as a bottom electrode, this method can create exciting new opportunities and potentially lead to technological advances for applications that benefit from ordered 3-D structures such as organic solar cells, sensors, batteries, and supercapacitors.

CONCLUSIONS

We have developed a one-step, facile solution-based method for growing highly ordered vertically aligned crystals for a variety of organic semiconductor by using graphene as a guiding substrate. The crystal densities and orientations can be readily controlled via solvent parameters. The resulting crystals are single crystalline in nature and exhibit uniform crystallographic and morphological orientations. High conductivity is achieved for the TANI crystals upon doping and is attributed to the ordered packing and their good contact quality with graphene. Furthermore, the vertical crystal arrays can be selectively grown into desired shapes by patterning the graphene substrate. These unique properties render the vertical crystals promising for potential applications in electronic and biomedical devices such as solar cells, supercapacitors, and sensors.

METHODS

Phenyl/phenyl-capped tetraaniline **1** and octaaniline **3** were synthesized by a condensation reaction under an inert atmosphere, and phenyl/amine-capped tetraaniline **2** was synthesized by a coupling reaction under ambient conditions, all via previously reported routes.[33] Sexithiophene **4** and bis(*N*-carbazolyl) biphenyl **5** were purchased from Sigma-Aldrich and used without further purification. The chemical structures of these compounds are shown in the Supporting Information as well as in Figures 3 and 7. CVD graphene was grown as previously reported.[55,56] Briefly, a 25 μm thick copper foil was electropolished, rolled into a tube and annealed under a 5/95% H_2/Ar environment at 1070 °C for 20 min. The temperature was then decreased to 1050 °C and methane was introduced for 30 min. The furnace was rapidly cooled and the resulting graphene film was wet transferred[55,56] using polylactic acid (Purac Biomaterials) onto a p^{+2}-SiO_2/Si wafer. Raman spectroscopy of the transferred graphene indicates it is a single-layer, and AFM characterization shows the graphene surface is rather smooth with an R_q of 0.233 nm (Figure S17).

Crystallization experiments were carried out in a covered Pyrex Petri dish under an ambient atmosphere. In brief, the covered Petri dish was partially filled with a nonsolvent (*e.g.*, *n*-hexane) for the molecule of interest. A piece of graphene-coated SiO_2/Si wafer was placed on a thick glass stage to raise it above the liquid level. A solution of the molecule was then dropped on the wafer. The vapor of the nonsolvent saturated the covered container and infiltrated into the solution on the wafer, leading to supersaturation followed by nucleation and crystallization (Figure S1).

Optical microscope and SEM images were collected on a Zeiss Axiotech Materials Microscope and JEOL-JSM-6700 field emission SEM, respectively. For the undoped samples, a 2 nm layer of platinum was sputtered onto the sample surface to reduce charging. Transmission electron microscope TEM samples were prepared by brushing a TEM grid against the wafer surface to mechanically transfer the crystals. TEM imaging and selected area electron diffraction (SAED) were performed on a FEI Tecnai G^2 TF20 TEM operated at 200 kV. SAED patterns were collected on multiple areas on each crystal, which showed identical patterns that confirmed their single crystalline nature. Multiple crystals were analyzed for each sample and reproducible results were obtained. Powder XRD spectra were collected on a Panalytical X'Pert Pro X-ray powder diffractometer using Cu Kα radiation with a wavelength of 0.15418 nm at a scan rate of 4.0° /min.

Tight-binding density functional theory (DFTB) calculations were performed to identify the preferred orientation of the TANI molecular precursors on graphene. The electronic structure of the graphene-TANI complex and stacking energy of TANI molecules were calculated to identify the potential significance of the vertical growth direction. The calculations were performed using a periodic graphene sheet with a vacuum layer. The binding energies and conformations of TANI molecules were calculated. The calculations are relatively large with more than 500 atoms in the computational domain and calculated using DFTB with sparse matrix parallelization as implemented in the DFTB+ code. The CHNO parameters used for the TANI were tested using higher-level DFT calculations as implemented in atom-centered all-electron DFT calculations using DMOL. The DFTB+ method was able to produce an accurate description of conjugation and bond distances for TANI molecules in comparison to higher-level DFT calculations.

Atomic force microscopy (AFM) was carried out using the Bruker Dimension Icon scanning probe microscope under ambient conditions. Topographic imaging was reproduced from multiple samples in the PeakForce Tapping mode using silicon nitride cantilevers (ScanAsyst-AIR, Bruker) with nominal spring constants of 0.4 N/m, first longitudinal resonance frequencies between 45 and 95 kHz, and nominal tip radii of ~2 nm. Images were processed by simple low-pass filtering and first-order plane fitting. Local *I*−*V* spectra were acquired by conductive AFM (cAFM) using the Bruker Extended TUNA applications module. Pt−Ir coated silicon cantilevers (SCM-PIC, Bruker) with calibrated spring constants between 0.12 and 0.15 N/m, first longitudinal resonance frequencies between 11.5 and 13 kHz, and nominal tip radii of <25 nm were used in PeakForce Tapping mode in order to provide quantitative control over the applied force, thereby reducing sample perturbations during the measurement. Bias voltage sweeps were applied to each sample with respect to a virtually ground cAFM

probe tip at a rate of 0.25 V/s over the range of interest, while maintaining a constant applied force throughout by means of the feedback loop. The reported $I-V$ characteristics were stable with repeated positive and negative bias sweeps and were the average of 20 $I-V$ curves taken at various positions on different crystals for each sample.

Graphene/TANI vertical crystal arrays/graphene sandwiched devices were fabricated by (1) depositing a strip of graphene, (2) defining Ti/Au contacts using a shadow mask followed by e-beam evaporation, (3) crystallizing TANI, and (4) depositing a top bilayer graphene electrode (Figure S14a). $I-V$ curves for these devices were obtained on a Lake Shore probe station.

The patterning of graphene was carried out using photolithography. AZ 5214 photoresist was spin-coated onto graphene-covered SiO_2/Si substrates at 3500 rpm. A photomask was aligned using a Karl Suss MA6 aligner followed by 6 s of UV exposure at an intensity of 8 mW. After developing the photoresist in the AZ Developer, the exposed graphene area was etched using an O_2 plasma in a Tegal Plasmaline Asher at 100 W for 60 s. The remaining photoresist was then stripped away using acetone followed by baking at 450 °C for 1 h under flowing Ar to remove the photoresist residue traces.

Conflict of Interest: The authors declare no competing financial interest.

Supporting Information Available: The Supporting Information is available free of charge on the ACS Publications website at DOI: 10.1021/acsnano.5b03465.

Additional characterization and measurement data (PDF)

Acknowledgment. The authors thank Rui Cheng and Henry D. Tran for helpful discussions, the UCLA Nanoelectronics Research Facility for cleanroom access, the Nano and Pico Characterization Lab and the Electron Imaging Center for Nanomachines at the California NanoSystems Institute for AFM and TEM usage, respectively. Financial support for this work has been provided by the Boeing Company (R.B.K.), NSF CAREER award 0956171 (X.D.), NSF CHE-1125054 (Y.R.), DOE award DE-EE006440 and DTRA grant HDTRA1-15-1-0034 (S.C.), a National Science Foundation-IGERT-MCTP Fellowship (M.T.Y.), a National Science Foundation-IGERT-CGI Fellowship (J.A.T.), and a National Science Foundation—Graduate Research Fellowship (Y.W.).

REFERENCES AND NOTES

1. Salleo, A. Charge Transport in Polymeric Transistors. *Mater. Today* **2007**, *10*, 38–45.
2. Wang, C. L.; Dong, H. L.; Hu, W. P.; Liu, Y. Q.; Zhu, D. B. Semiconducting π-Conjugated Systems in Field-Effect Transistors: A Material Odyssey of Organic Electronics. *Chem. Rev.* **2012**, *112*, 2208–2267.
3. Sondergaard, R.; Hosel, M.; Angmo, D.; Larsen-Olsen, T. T.; Krebs, F. C. Roll-to-Roll Fabrication of Polymer Solar Cells. *Mater. Today* **2012**, *15*, 36–49.
4. Minemawari, H.; Yamada, T.; Matsui, H.; Tsutsumi, J.; Haas, S.; Chiba, R.; Kumai, R.; Hasegawa, T. Inkjet Printing of Single-Crystal Films. *Nature* **2011**, *475*, 364–367.
5. Diao, Y.; Tee, B. C. K.; Giri, G.; Xu, J.; Kim, D. H.; Becerril, H. A.; Stoltenberg, R. M.; Lee, T. H.; Xue, G.; Mannsfeld, S. C. B.; Bao, Z. N. Solution Coating of Large-Area Organic Semiconductor Thin Films with Aligned Single-Crystalline Domains. *Nat. Mater.* **2013**, *12*, 665–671.
6. Huang, Y.; Duan, X. F.; Wei, Q. Q.; Lieber, C. M. Directed Assembly of One-Dimensional Nanostructures into Functional Networks. *Science* **2001**, *291*, 630–633.
7. Liu, S.; Wang, W. M.; Briseno, A. L.; Mannsfeld, S. C. B.; Bao, Z. Controlled Deposition of Crystalline Organic Semiconductors for Field-Effect-Transistor Applications. *Adv. Mater.* **2009**, *21*, 1217–1232.
8. Fan, Z. Y.; Razavi, H.; Do, J. W.; Moriwaki, A.; Ergen, O.; Chueh, Y. L.; Leu, P. W.; Ho, J. C.; Takahashi, T.; Reichertz, L. A.; Neale, S.; Yu, K.; Wu, M.; Ager, J. W.; Javey, A. Three-Dimensional Nanopillar-Array Photovoltaics on Low-Cost and Flexible Substrates. *Nat. Mater.* **2009**, *8*, 648–653.
9. Greene, L. E.; Law, M.; Tan, D. H.; Montano, M.; Goldberger, J.; Somorjai, G.; Yang, P. D. General Route To Vertical ZnO Nanowire Arrays Using Textured ZnO Seeds. *Nano Lett.* **2005**, *5*, 1231–1236.
10. Zhao, Y. S.; Wu, J. S.; Huang, J. X. Vertical Organic Nanowire Arrays: Controlled Synthesis and Chemical Sensors. *J. Am. Chem. Soc.* **2009**, *131*, 3158–3159.
11. Ng, H. T.; Han, J.; Yamada, T.; Nguyen, P.; Chen, Y. P.; Meyyappan, M. Single Crystal Nanowire Vertical Surround-Gate Field-Effect Transistor. *Nano Lett.* **2004**, *4*, 1247–1252.
12. Mariani, G.; Wang, Y.; Wong, P. S.; Lech, A.; Hung, C. H.; Shapiro, J.; Prikhodko, S.; El-Kady, M.; Kaner, R. B.; Huffaker, D. L. Three-Dimensional Core-Shell Hybrid Solar Cells *via* Controlled *in Situ* Materials Engineering. *Nano Lett.* **2012**, *12*, 3581–3586.
13. Robinson, J. T.; Jorgolli, M.; Shalek, A. K.; Yoon, M. H.; Gertner, R. S.; Park, H. Vertical Nanowire Electrode Arrays As a Scalable Platform for Intracellular Interfacing to Neuronal Circuits. *Nat. Nanotechnol.* **2012**, *7*, 180–184.
14. Xu, S.; Qin, Y.; Xu, C.; Wei, Y. G.; Yang, R. S.; Wang, Z. L. Self-Powered Nanowire Devices. *Nat. Nanotechnol.* **2010**, *5*, 366–373.
15. Tomioka, K.; Yoshimura, M.; Fukui, T. A III-V Nanowire Channel on Silicon for High-Performance Vertical Transistors. *Nature* **2012**, *488*, 189–193.
16. Miller, J. R.; Outlaw, R. A.; Holloway, B. C. Graphene Double-Layer Capacitor with ac Line-Filtering Performance. *Science* **2010**, *329*, 1637–1639.
17. Thurn-Albrecht, T.; Schotter, J.; Kastle, C. A.; Emley, N.; Shibauchi, T.; Krusin-Elbaum, L.; Guarini, K.; Black, C. T.; Tuominen, M. T.; Russell, T. P. Ultrahigh-Density Nanowire Arrays Grown in Self-Assembled Diblock Copolymer Templates. *Science* **2000**, *290*, 2126–2129.
18. Hu, J. C.; Clark, K. W.; Hayakawa, R.; Li, A. P.; Wakayama, Y. Enhanced Electrical Conductivity in Poly(3-hexylthiophene)/Fluorinated Tetracyanoquinodimethane Nanowires Grown with a Porous Alumina Template. *Langmuir* **2013**, *29*, 7266–7270.
19. Singh, V.; Bougher, T. L.; Weathers, A.; Cai, Y.; Bi, K.; Pettes, M. T.; McMenamin, S. A.; Lv, W.; Resler, D. P.; Gattuso, T. R.; et al. High Thermal Conductivity of Chain Oriented Amorphous Polythiophene. *Nat. Nanotechnol.* **2014**, *9*, 384–390.
20. Xiao, K.; Deng, W.; Keum, J. K.; Yoon, M.; Vlassiouk, I. V.; Clark, K. W.; Li, A. P.; Kravchenko, I. I.; Gu, G.; Payzant, E. A.; et al. Surface-Induced Orientation Control of CuPc Molecules for the Epitaxial Growth of Highly Ordered Organic Crystals on Graphene. *J. Am. Chem. Soc.* **2013**, *135*, 3680–3687.
21. Wang, Q. H.; Hersam, M. C. Room-Temperature Molecular-Resolution Characterization of Self-Assembled Organic Monolayers on Epitaxial Graphene. *Nat. Chem.* **2009**, *1*, 206–211.
22. Nguyen, N. N.; Jo, S. B.; Lee, S. K.; Sin, D. H.; Kang, B. Atomically Thin Epitaxial Template for Organic Crystal Growth Using Graphene with Controlled Surface Wettability. *Nano Lett.* **2015**, *15*, 2474–2484.
23. Balzer, F.; Henrichsen, H. H.; Klarskov, M. B.; Booth, T. J.; Sun, R.; Parisi, J.; Schiek, M.; Boggild, P. Directed Self-Assembled Crystalline Oligomer Domains on Graphene and Graphite. *Nanotechnology* **2014**, *25*, 035602.
24. Lee, W. H.; Park, J.; Sim, S. H.; Lim, S.; Kim, K. S.; Hong, B. H.; Cho, K. Surface-Directed Molecular Assembly of Pentacene on Monolayer Graphene for High-Performance Organic Transistors. *J. Am. Chem. Soc.* **2011**, *133*, 4447–4454.
25. Salzmann, I.; Moser, A.; Oehzelt, M.; Breuer, T.; Feng, X. L.; Juang, Z. Y.; Nabok, D.; Della Valle, R. G.; Duhm, S.; Heimel, G.; et al. Epitaxial Growth of π-Stacked Perfluoropentacene on Graphene-Coated Quartz. *ACS Nano* **2012**, *6*, 10874–10883.
26. Simbrunner, C. Epitaxial Growth of Sexi-Thiophene and Para-Hexaphenyl and Its Implications for the Fabrication of Self-Assembled Lasing Nano-Fibres. *Semicond. Sci. Technol.* **2013**, *28*, 53001.

27. Kim, D. H.; Lee, H. S.; Shin, H. J.; Bae, Y. S.; Lee, K. H.; Kim, S. W.; Choi, D.; Choi, J. Y. Graphene Surface Induced Specific Self-Assembly of Poly(3-Hexylthiophene) for Nanohybrid Optoelectronics: From First-Principles Calculation to Experimental Characterizations. *Soft Matter* **2013**, *9*, 5355–5360.
28. Skrypnychuk, V.; Boulanger, N.; Yu, V. Enhanced Vertical Charge Transport in a Semiconducting P3HT Thin Film on Single Layer Graphene. *Adv. Funct. Mater.* **2015**, *25*, 664–670.
29. Zhong, S.; Zhong, J. Q.; Mao, H. Y.; Wang, R.; Wang, Y.; Qi, D. C.; Loh, K. P.; Wee, A. T. S.; Chen, Z. K.; Chen, W. CVD Graphene As Interfacial Layer to Engineer the Organic Donor Acceptor Heterojunction Interface Properties. *ACS Appl. Mater. Interfaces* **2012**, *4*, 3134–3140.
30. Kim, K.; Lee, T. H.; Santos, E. J. G.; Jo, P. S.; Salleo, A.; Nishi, Y.; Bao, Z. Structural and Electrical Investigation of C_{60}-Graphene Vertical Heterostructures. *ACS Nano* **2015**, *9* (6), 5922–5928.
31. Zhang, Y.; Diao, Y.; Lee, H.; Mirabito, T. J.; Johnson, R. W.; Puodziukynaite, E.; John, J.; Carter, K. R.; Emrick, T.; Mannsfeld, S. C. B.; Briseno, A. L. Intrinsic and Extrinsic Parameters for Controlling the Growth of Organic Single-Crystalline Nanopillars in Photovoltaics. *Nano Lett.* **2014**, *14*, 5547–5554.
32. Wang, Y.; Liu, J. L.; Tran, H. D.; Mecklenburg, M.; Guan, X. N.; Stieg, A. Z.; Regan, B. C.; Martin, D. C.; Kaner, R. B. Morphological and Dimensional Control *via* Hierarchical Assembly of Doped Oligoaniline Single Crystals. *J. Am. Chem. Soc.* **2012**, *134*, 9251–9262.
33. Wang, Y.; Tran, H. D.; Liao, L.; Duan, X. F.; Kaner, R. B. Nanoscale Morphology, Dimensional Control, and Electrical Properties of Oligoanilines. *J. Am. Chem. Soc.* **2010**, *132*, 10365–10373.
34. Li, D.; Huang, J. X.; Kaner, R. B. Polyaniline Nanofibers: A Unique Polymer Nanostructure for Versatile Applications. *Acc. Chem. Res.* **2009**, *42*, 135–145.
35. Li, X. S.; Cai, W. W.; An, J. H.; Kim, S.; Nah, J.; Yang, D. X.; Piner, R.; Velamakanni, A.; Jung, I.; Tutuc, E.; et al. Large-Area Synthesis of High-Quality and Uniform Graphene Films on Copper Foils. *Science* **2009**, *324*, 1312–1314.
36. Novoselov, K. S.; Geim, A. K.; Morozov, S. V.; Jiang, D.; Zhang, Y.; Dubonos, S. V.; Grigorieva, I. V.; Firsov, A. A. Electric Field Effect in Atomically Thin Carbon Films. *Science* **2004**, *306*, 666–669.
37. Tung, V. C.; Allen, M. J.; Yang, Y.; Kaner, R. B. High-Throughput Solution Processing of Large-Scale Graphene. *Nat. Nanotechnol.* **2009**, *4*, 25–29.
38. Strong, V.; Dubin, S.; El-Kady, M. F.; Lech, A.; Wang, Y.; Weiller, B. H.; Kaner, R. B. Patterning and Electronic Tuning of Laser Scribed Graphene for Flexible All-Carbon Devices. *ACS Nano* **2012**, *6*, 1395–1403.
39. Novoselov, K. S.; Fal'ko, V. I.; Colombo, L.; Gellert, P. R.; Schwab, M. G.; Kim, K. A Roadmap for Graphene. *Nature* **2012**, *490*, 192–200.
40. Smallwood, I. M. *Handbook of Organic Solvent Properties*; Elsevier: New York, 1996.
41. Li, Z. T.; Wang, Y. J.; Kozbial, A.; Shenoy, G.; Zhou, F.; McGinley, R.; Ireland, P.; Morganstein, B.; Kunkel, A.; Surwade, S. P.; et al. Effect of Airborne Contaminants on the Wettability of Supported Graphene and Graphite. *Nat. Mater.* **2013**, *12*, 925–931.
42. Vekilov, P. G. Nucleation. *Cryst. Growth Des.* **2010**, *10*, 5007–5019.
43. Macdiarmid, A. G.; Epstein, A. J. The Concept of Secondary Doping As Applied to Polyaniline. *Synth. Met.* **1994**, *65*, 103–116.
44. Ma, Z. Y.; Geng, Y. H.; Yan, D. H. Extended-Chain Lamellar Packing of Poly(3-butylthiophene) in Single Crystals. *Polymer* **2007**, *48*, 31–34.
45. Xiao, X. L.; Hu, Z. J.; Wang, Z. B.; He, T. B. Study on the Single Crystals of Poly(3-octylthiophene) Induced by Solvent-Vapor Annealing. *J. Phys. Chem. B* **2009**, *113*, 14604–14610.
46. Kim, D. H.; Han, J. T.; Park, Y. D.; Jang, Y.; Cho, J. H.; Hwang, M.; Cho, K. Single-Crystal Polythiophene Microwires Grown by Self-Assembly. *Adv. Mater.* **2006**, *18*, 719–723.
47. Nardes, A. M.; Kemerink, M.; Janssen, R. A. J. Anisotropic Hopping Conduction in Spin-Coated PEDOT: PSS Thin Films. *Phys. Rev. B* **2007**, *76*, 085208.
48. Sundar, V. C.; Zaumseil, J.; Podzorov, V.; Menard, E.; Willett, R. L.; Someya, T.; Gershenson, M. E.; Rogers, J. A. Elastomeric Transistor Stamps: Reversible Probing Of Charge Transport In Organic Crystals. *Science* **2004**, *303*, 1644–1646.
49. Mayer, A.; Scully, S.; Hardin, B.; Rowell, M.; McGehee, M. Polymer-Based Solar Cells. *Mater. Today* **2007**, *10*, 28–33.
50. Cui, L. F.; Ruffo, R.; Chan, C. K.; Peng, H. L.; Cui, Y. Crystalline-Amorphous Core-Shell Silicon Nanowires for High Capacity and High Current Battery Electrodes. *Nano Lett.* **2009**, *9*, 491–495.
51. MacDiarmid, A. G.; Zhou, Y.; Feng, J. Oligomers and Isomers: New Horizons in Poly-Anilines. *Synth. Met.* **1999**, *100*, 131–140.
52. Briseno, A. L.; Mannsfeld, S. C.; Ling, M. M.; Liu, S.; Tseng, R. J.; Reese, C.; Roberts, M. E.; Yang, Y.; Wudl, F.; Bao, Z. Patterning Organic Single-Crystal Transistor Arrays. *Nature* **2006**, *444*, 913–7.
53. De Vusser, S.; Steudel, S.; Myny, K.; Genoe, J.; Heremans, P. Integrated Shadow Mask Method for Patterning Small Molecule Organic Semiconductors. *Appl. Phys. Lett.* **2006**, *88*, 103501.
54. Menard, E.; Meitl, M. A.; Sun, Y. G.; Park, J. U.; Shir, D. J. L.; Nam, Y. S.; Jeon, S.; Rogers, J. A. Micro- and Nanopatterning Techniques for Organic Electronic and Optoelectronic Systems. *Chem. Rev.* **2007**, *107*, 1117–1160.
55. Chen, S. S.; Ji, H. X.; Chou, H.; Li, Q. Y.; Li, H. Y.; Suk, J. W.; Piner, R.; Liao, L.; Cai, W. W.; Ruoff, R. S. Millimeter-Size Single-Crystal Graphene by Suppressing Evaporative Loss of Cu During Low Pressure Chemical Vapor Deposition. *Adv. Mater.* **2013**, *25*, 2062–2065.
56. Li, X. S.; Zhu, Y. W.; Cai, W. W.; Borysiak, M.; Han, B. Y.; Chen, D.; Piner, R. D.; Colombo, L.; Ruoff, R. S. Transfer of Large-Area Graphene Films for High-Performance Transparent Conductive Electrodes. *Nano Lett.* **2009**, *9*, 4359–4363.